Archive of Applied Mechanics 68 (1998) 247–258 © Springer-Verlag 1998

# Crack shielding and material deterioration in damaged materials: an antiplane shear fracture problem

**Z. H. Jin, R. C. Batra**



**Summary** A simple damage evolution model is proposed for a quasibrittle material in the framework of continuum damage mechanics. The model is used to obtain a closed form solution for a mode-III stationary crack under small scale damage conditions. It is found that the crack tip stress intensity factor is reduced, i.e., the crack is shielded by the damage. However, this shielding effect is completely offset by the material deterioration caused by the damage. It also holds for steady state crack growth. When the most effective shielding is reached for the stationary crack, the zone dominated by the stress intensity factor shrinks to the crack tip. The results for the antiplane shear problem should shed some light on the in-plane fracture problem.

**Keywords** Stress intensity factor, damage, material degradation, fracture

## 1 Introduction

Quasibrittle materials such as concrete and ceramics do not deform as ideal elastic materials. For example, they are damaged by severe loads, which leads to their nonlinear constitutive behaviour. For a polycrystalline material, it has been assumed [1] that the material is not damaged and the classical Hooke's law applies until an effective stress reaches a threshold value. Beyond the threshold stress, the material is progressively damaged by microcracking, and when the effective stress reaches a critical value, the saturation stress, the material damage saturates and the stress–strain curve is again a straight line with a lower modulus, or the saturation modulus. This was also assumed in subsequent studies [2–4] on crack shielding by microcracking in ceramics. Based on the aforestated assumptions, phenomenological models have been developed and applied to crack problems. It has been found that the stress intensity factor at a mode-I crack tip is significantly reduced [2–4]. Several other constitutive models have also been proposed for quasibrittle materials [5–7]. Though damage around a crack tip may reduce the stress intensity factor, it also deteriorates the material. Based on the estimates of the elastic moduli of a microcracked solid, the microcrack density and the fraction of microcracked facets, and micromechanical analyses it has been shown [1] that the damage, in the form of microcracking, mainly distributed ahead of the crack tip does not contribute to the toughness of the material. By assuming an array of coplanar microcracks ahead of a macrocrack, using a cohesive model, and estimating the microcrack density near the main crack tip, the crack shielding is shown to be nearly counterbalanced by the toughness degradation [9].

Antiplane shear fields around a stationary crack and around a steadily growing crack in a damaged material are studied herein, and a simple damage evolution model is proposed in the framework of continuum damage mechanics [10, 11]. Closed form solutions for stresses and strains in the damaged material are obtained, and the effect of damage on both crack shielding and material deterioration is delineated.

*Received 4 August 1997; accepted for publication 7 October 1997*

Z. H. Jin, R. C. Batra
Department of Engineering Science and Mechanics,
Virginia Polytechnic Institute and State University,
Blacksburg, VA 24061–0219, USA

## 2
## Basic equations of a damaged material under antiplane shear

Consider antiplane shear (mode III) deformations around a stationary crack in a damaged material, and neglect its permanent deformations. We also neglect the anisotropic effects induced by damage since this is less significant for crack shielding than the effect of the reduction in the modulus. The consideration of material anisotropy will generally exclude antiplane shear deformations. With these assumptions, the constitutive equation of brittle damaged materials is [10, 11]



$$\varepsilon_{ij} = \frac{1+\nu_0}{E_0(1-\omega)}\sigma_{ij} - \frac{\nu_0}{E_0(1-\omega)}\sigma_{kk}\delta_{ij} \tag{1}$$

where $\varepsilon_{ij}$ are infinitesimal strains, $\sigma_{ij}$ stresses, $E_0$ and $\nu_0$ Young's modulus and Poisson's ratio of the undamaged material, and $\omega$ is a scalar internal variable that characterizes damage. The variable $\omega$ is zero for undamaged materials, and can not be greater than one for fully damaged materials.

Following the damage evolution criterion for a quasibrittle concrete [12], we assume that

$$\dot{\omega} = \begin{cases} 0, & \text{when either } f = 0 \text{ and } \dot{f} < 0, \text{ or } f < 0, \\ \lambda(\tilde{\sigma})\langle\tilde{\sigma}\rangle_+, & \text{when } f = 0 \text{ and } \dot{f} = 0 \ , \end{cases} \tag{2a}$$

$$f(\tilde{\sigma}, \omega) = \tilde{\sigma} - K(\omega), \quad K(0) = \sigma_c \ , \tag{2b}$$

where a superimposed dot denotes the material time derivative, $\tilde{\sigma}$ is an equivalent stress given by

$$\tilde{\sigma} = \left(\langle\sigma_1\rangle_+^2 + \langle\sigma_2\rangle_+^2 + \langle\sigma_3\rangle_+^2\right)^{1/2} \ , \tag{3}$$

$\sigma_i$ $(i = 1, 2, 3)$ are the principal stresses, and the symbol $\langle\ \rangle_+$ is defined by

$$\langle\sigma_i\rangle_+ = \begin{cases} 0, & \sigma_i < 0 \ , \\ \sigma_i, & \sigma_i \geq 0 \ . \end{cases} \tag{4}$$

In Eq. (2), $\sigma_c$ is the threshold stress and $\lambda(\tilde{\sigma})$ can be determined from a simple uniaxial test. For proportional loading, Eq. (2) can be integrated to obtain the following equation for damage.

$$\omega = \Lambda(\tilde{\sigma}), \ \Lambda(\tilde{\sigma}) = \int_{\sigma_c}^{\tilde{\sigma}} \lambda(\sigma)\mathrm{d}\sigma \ . \tag{5}$$

A typical uniaxial stress–strain curve [1–4] of a damaged material is shown in Fig. 1 where $\sigma_s$ is the saturation stress, i.e., for $\sigma > \sigma_s$, the damage is saturated and no further damage occurs. It can be seen from Fig. 1 and Eqs. (1) and (5) that in the initial elastic stage

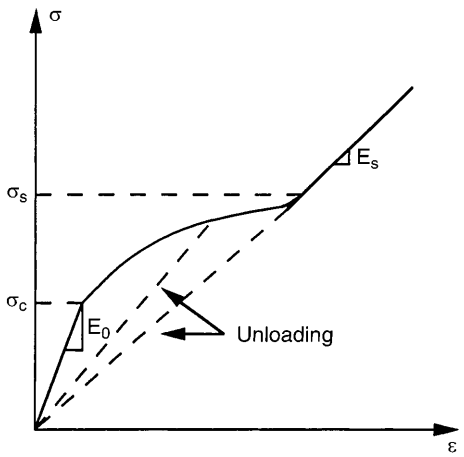


**Fig. 1.** Uniaxial stress–strain curve of a damaged material

$$\Lambda(\tilde{\sigma}) = 0 \quad (\tilde{\sigma} \leq \sigma_0) \ ,$$

and in the saturation stage

$$\Lambda(\tilde{\sigma}) = 1 - \frac{E_s}{E_0} \quad (\tilde{\sigma} \geq \sigma_s) \ .$$

Here, $E_s$ is the modulus in the saturation stage and $E_s < E_0$.

We now deduce equations for antiplane shear deformations. Antiplane shear models may not be very appropriate for brittle materials. However, their mathematical simplicity allows closed form solutions which may help understand the in-plane fracture problems. For antiplane shear deformations, the nonvanishing unknowns are the longitudinal displacement $w$, shear stresses $\tau_x = \sigma_{13}$ and $\tau_y = \sigma_{23}$, shear strains $\gamma_x = 2\varepsilon_{13}$ and $\gamma_y = 2\varepsilon_{23}$ and the damage $\omega$. They satisfy the equilibrium equation,



$$\frac{\partial \tau_x}{\partial x} + \frac{\partial \tau_y}{\partial y} = 0 \ ; \tag{6}$$

the strain-displacement relations,

$$(\gamma_x, \gamma_y) = \left( \frac{\partial w}{\partial x}, \frac{\partial w}{\partial y} \right) \ , \tag{7}$$

and the constitutive equations reduced from Eq. (1)

$$(\gamma_x, \gamma_y) = \frac{1}{\mu_0 (1 - \omega)} (\tau_x, \tau_y) \ , \tag{8}$$

where $\mu_0$ is the shear modulus of the undamaged material. The displacement, $w$, can be eliminated from Eq. (7) to obtain the compatibility condition,

$$\frac{\partial \gamma_y}{\partial x} - \frac{\partial \gamma_x}{\partial y} = 0 \ . \tag{9}$$

For antiplane shear, the principal stresses $\sigma_i$ are

$$\begin{aligned} &\sigma_1 = \tau, \quad \sigma_2 = 0, \quad \sigma_3 = -\tau, \\ &\tau = \left( \tau_x^2 + \tau_y^2 \right)^{1/2} \ . \end{aligned} \tag{10}$$

Substitution from Eq. (10) into definition (3) yields

$$\tilde{\sigma} = \tau \tag{11}$$

Equations (5), (8) and (11) imply that

$$(\gamma_x, \gamma_y) = \frac{1}{\mu_0 [1 - \Lambda(\tau)]} (\tau_x, \tau_y) \ , \tag{12a}$$

and, consequently

$$\gamma = \frac{\tau}{\mu_0 [1 - \Lambda(\tau)]} \ , \tag{12b}$$

where

$$\gamma = \left( \gamma_x^2 + \gamma_y^2 \right)^{1/2} \ . \tag{13}$$

We write Eq. (12) in the alternative form as

$$(\tau_x, \tau_y) = \frac{\tau(\gamma)}{\gamma}(\gamma_x, \gamma_y) \tag{14}$$

where

$$\frac{\tau(\gamma)}{\tau_c} = \begin{cases} \frac{\gamma}{\gamma_c}, & 0 \le \gamma \le \gamma_c \ , \\ f\left(\frac{\gamma}{\gamma_c}\right), & \gamma_c \le \gamma \le \gamma_s \ , \\ \frac{\mu_s}{\mu_0}\frac{\gamma}{\gamma_c}, & \gamma \ge \gamma_s \ , \end{cases} \tag{15}$$



in which $\tau_c = \sigma_c, \tau_s = \sigma_s, \gamma_c = \tau_c/\mu_0, \gamma_s = \tau_s/\mu_s$, and $\mu_s$ is the shear modulus in the saturation stage. We assume that

$$f\left(\frac{\gamma}{\gamma_c}\right) = \left(\frac{\gamma}{\gamma_c}\right)^N \tag{16}$$

with power $N$ determined by

$$\left(\frac{\gamma_s}{\gamma_c}\right)^N = \left(\frac{\tau_s}{\tau_c}\right) \tag{17}$$

which results from the continuity requirement of the stress–strain curve.

The damage $\omega(\tau)$ can be obtained from Eqs. (5), (11), (12b) and (15)

$$\omega(\tau) = \begin{cases} 0, & 0 \le \tau \le \tau_c \ , \\ 1 - \left(\frac{\tau}{\tau_c}\right)^{\frac{N-1}{N}}, & \tau_c \le \tau \le \tau_s \ , \\ 1 - \frac{\mu_s}{\mu_0}, & \tau \ge \tau_s \ . \end{cases} \tag{18}$$

## 3
## A solution of the small-scale damage problem

We seek solutions of a crack problem involving small-scale damage; we thus consider a semi-infinite crack in an infinite body as shown in Fig. 2. The boundary conditions for the crack problem are

$$w = 0, \quad 0 < \frac{x}{r_0} < \infty, \quad y = 0 \ , \tag{19}$$

$$\tau_y = 0, \quad -\infty < \frac{x}{r_0} < 0, \quad y = 0 \ , \tag{20}$$

and the matching conditions are

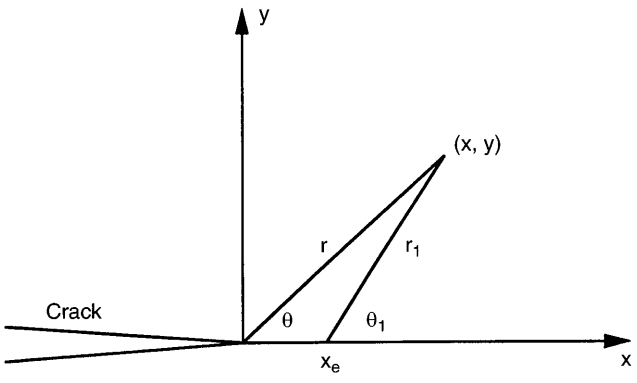


**Fig. 2.** A semi-infinite crack in an infinite body for a small scale damage problem

$$\omega \to 0, \quad w \to 2\frac{K^o_{\mathrm{III}}}{\mu_0}\sqrt{\frac{r}{2\pi}}\sin\frac{\theta}{2}, \quad (\tau_x, \tau_y) \to \frac{K^o_{\mathrm{III}}}{\sqrt{2\pi r}}\left(-\sin\frac{\theta}{2}, \cos\frac{\theta}{2}\right) \quad \text{as } \frac{r}{r_0} \to \infty, \ 0 \le \theta \le \pi \ . \tag{21}$$

Here, $K^o_{\mathrm{III}}$ is the applied mode-III stress intensity factor. In Eqs. (19)–(21), $r_0$ is a reference length of the crack tip damage zone, and is given by

$$r_0 = \frac{(K^o_{\mathrm{III}})^2}{2\pi\tau_c^2} \ . \tag{22}$$



By using the hodograph transformation method [13, 14], the basic equations in the strain plane are

$$\frac{\partial^2\psi}{\partial\gamma^2} + \frac{1}{\gamma}\frac{\partial\psi}{\partial\gamma} + \frac{1}{\gamma^2}\frac{\partial^2\psi}{\partial\phi^2} = 0, \ \text{either } 0 < \gamma < 1 \text{ or } \gamma > \beta, \ 0 < \phi < \frac{\pi}{2} \ , \tag{23}$$

in the undamaged and damage saturated regions, and

$$\frac{1}{N}\frac{\partial^2\psi}{\partial\gamma^2} + \frac{1}{\gamma}\frac{\partial\psi}{\partial\gamma} + \frac{1}{\gamma^2}\frac{\partial^2\psi}{\partial\phi^2} = 0, \quad 1 < \gamma < \beta, \ 0 < \phi < \frac{\pi}{2} \ , \tag{24}$$

in the progressively damaged region. In Eqs. (23) and (24), $\psi$ is a function of strains defined by

$$x - iy = -e^{i\phi}\left(\frac{1}{\gamma}\frac{\partial\psi}{\partial\phi} + i\frac{\partial\psi}{\partial\gamma}\right) \tag{25}$$

and $\gamma$ and $\phi$ are related to $\gamma_x$ and $\gamma_y$ by

$$(\gamma_x, \gamma_y) = \gamma(-\sin\phi, \cos\phi) \ . \tag{26}$$

We note that $\psi, \gamma, \gamma_x$ and $\gamma_y$ in Eqs. (23)–(26) have been normalized by $\gamma_c$, and hence $\beta$ in Eqs. (23) and (24) is given by

$$\beta = \frac{\gamma_s}{\gamma_c} \tag{27}$$

The boundary conditions on $\psi$ are

$$\psi = 0, \ \phi = 0, \ \gamma > 0 \ , \tag{28a}$$

$$\frac{\partial\psi}{\partial\phi} = 0, \ \phi = \frac{\pi}{2}, \ \gamma > 0 \ , \tag{28b}$$

and

$$\psi \to -r_0\frac{\sin\phi}{\gamma}, \ \gamma \to 0 \ , \tag{29a}$$

$$\frac{\partial\psi}{\partial\gamma} \to 0, \ \frac{1}{\gamma}\frac{\partial\psi}{\partial\phi} \to 0, \ \gamma \to \infty \ . \tag{29b}$$

In addition to conditions (28) and (29), we also have the following continuity requirements on the boundaries between different regions

$$[\psi]_{\gamma=1} = \left[\frac{\partial\psi}{\partial\gamma}\right]_{\gamma=1} = 0 \ , \tag{30}$$

$$[\psi]_{\gamma=\beta} = \left[\frac{\partial\psi}{\partial\gamma}\right]_{\gamma=\beta} = 0 \ , \tag{31}$$

where $[\psi]_\Gamma$ represents the jump of $\psi$ across the curve $\Gamma$.

The solutions of Eqs. (23) and (24) subject to conditions (28)–(31) is

$$\psi = r_0\left\{\frac{1-N}{1+N}[\beta^{-(1+N)} - 1]\gamma - \frac{1}{\gamma}\right\}\sin\phi \tag{32}$$

in the undamaged region ($\gamma < 1$),



$$\psi = \frac{r_0}{1+N}[(1-N)\beta^{-(1+N)}\gamma - 2\gamma^{-N}]\sin\phi \tag{33}$$

in the progressively damaged region ($1 < \gamma < \beta$), and

$$\psi = -r_0\beta^{1-N}\frac{\sin\phi}{\gamma} \tag{34}$$

in the damage saturation region ($\gamma > \beta$).

By substituting solutions (32)–(34) into definition (25), and using Eqs. (26) and (14)–(17), we obtain the following explicit solutions for strain and stress fields:

$$\gamma = \frac{K^o_{\mathrm{III}}}{\tau_c\sqrt{2\pi r_1}}, \quad \phi = \frac{1}{2}\theta_1 \ , \tag{35a,b}$$

$$(\gamma_x, \gamma_y) = \frac{K^o_{\mathrm{III}}}{\tau_c\sqrt{2\pi r_1}}\left(-\sin\frac{\theta_1}{2}, \cos\frac{\theta_1}{2}\right) \ , \tag{35c}$$

$$(\tau_x, \tau_y) = \frac{K^o_{\mathrm{III}}}{\sqrt{2\pi r_1}}\left(-\sin\frac{\theta_1}{2}, \cos\frac{\theta_1}{2}\right) \ , \tag{35d}$$

in the undamaged region ($\gamma \leqslant 1$),

$$\gamma = \left\{\frac{1+N}{4N}\sqrt{\left[(1+N)\frac{x}{r_0} + (1-N)\beta^{-(1+N)}\right]^2 + 4N\left(\frac{y}{r_0}\right)^2} - \frac{1-N^2}{4N}\frac{x}{r_0} - \frac{(1-N)^2}{4N}\beta^{-(1+N)}\right\}^{\frac{-1}{1+N}} , \tag{36a}$$

$$\phi = \frac{1}{2}\tan^{-1}\left\{\frac{y}{x - \frac{1-N}{1+N}r_0\left[\gamma^{-(1+N)} - \beta^{-(1+N)}\right]}\right\} \ , \tag{36b}$$

$$(\gamma_x, \gamma_y) = \gamma(-\sin\phi, \cos\phi) \ , \tag{36c}$$

$$(\tau_x, \tau_y) = \tau_c\gamma^N(-\sin\phi, \cos\phi) \ , \tag{36d}$$

in the progressively damaged region ($1 < \gamma < \beta$), and

$$\gamma = \frac{\mu_0}{\mu_s}\frac{K_{\mathrm{tip}}}{\tau_c\sqrt{2\pi r}}, \quad \phi = \frac{1}{2}\theta \ , \tag{37a,b}$$

$$(\gamma_x, \gamma_y) = \frac{\mu_0}{\mu_s}\frac{K_{\mathrm{tip}}}{\tau_c\sqrt{2\pi r}}\left(-\sin\frac{\theta}{2}, \cos\frac{\theta}{2}\right) \ , \tag{37c}$$

$$(\tau_x, \tau_y) = \frac{K_{\text{tip}}}{\sqrt{2\pi r}}\left(-\sin\frac{\theta}{2}, \cos\frac{\theta}{2}\right) \ , \tag{37d}$$

in the damage saturation region ($\gamma \geq \beta$). In Eqs. (35)–(37), $r_1$ and $\theta_1$ are polar coordinates defined by (see Fig. 2)

$$r_1 \cos\theta_1 = x - x_e, \quad r_1 \sin\theta_1 = y \ , \tag{38}$$

where

$$x_e = \frac{1-N}{1+N} r_0 \left[1 - \beta^{-(1+N)}\right] \ , \tag{39}$$



and $K_{\text{tip}}$ is the crack tip mode-III stress intensity factor given by

$$K_{\text{tip}} = \sqrt{\frac{\mu_s}{\mu_0}} K^o_{\text{III}} \ . \tag{40}$$

Since $\mu_s < \mu_0$ (the material is weakened by damage), the stress intensity factor at the crack tip is reduced, i.e., the crack is shielded by the crack tip damage effect. Equation (40) agrees qualitatively with the result for the mode-I crack problem [2, 3].

Several remarks can be made for solutions (35)–(40). First, lines of constant strain magnitude ($\gamma = \text{const.}$) are circles in all regions. Hence, boundaries separating different regions are circles. The boundary $\Gamma_d$, between the damaged region and the progressively damaged region is obtained by setting $\gamma = 1$ in either Eq. (35a) or (36a)

$$\Gamma_d\text{: } (x - x_e)^2 + y^2 = r_0^2 \ , \tag{41}$$

The boundary, $\Gamma_s$, separating the progressively damaged and saturated damaged zones is described by

$$\Gamma_s\text{: } x^2 + y^2 = r_0^2 \beta^{-2(1+N)} = r_s^2 \left(\frac{\mu_s}{\mu_0}\right)^2 \ , \tag{42a}$$

where

$$r_s = \frac{(K^o_{\text{III}})^2}{2\pi\tau_s^2} \ . \tag{42b}$$

It can be easily shown that $r_0^2 \beta^{-2(1+N)} < \min\{r_0^2, (r_0 - x_e)^2\}$ when $\tau_s > \tau_c$. Hence, the damage saturation zone is completely encompassed by the progressively damaged zone. Figure 3 shows the geometry of damage around the crack tip. Second, the square root singular solution (37) holds in the entire saturation region. But this is generally not true for in-plane crack problems for which the singular solution is only an asymptotic solution in the saturation region. Third, the constitutive equation (14) with (13) and (15) is valid for proportional deformations. We can see from Eq. (37) that the proportional deformation condition is fulfilled in the damage saturation region where $\phi$ is independent of the applied load $K^o_{\text{III}}$. While the fracture behavior is controlled by the process in the crack tip saturation zone, we can expect that the constitutive equation (14) is adequate for stationary crack problems. Finally, though the crack tip stress intensity factor decreases with a decrease in $\mu_s/\mu_0$, the radius of the damage saturation zone dominated by the stress intensity factor also decreases with a decrease in $\mu_s/\mu_0$. In fact, the radius becomes vanishingly small when $\mu_s/\mu_0$ goes to zero as indicated by Eq. (42).

We have seen that the crack is shielded by damage. However, damage also degrades the material and may reduce its resistance to crack growth. In continuum damage mechanics, material failure is described by $\omega = 1$. In the present damage model, however, damage saturates at $\omega = 1 - \mu_s/\mu_0$ for large values of stress $\tau$. Hence, the material failure may still be described by the conventional fracture mechanics approach. Since the isotropic damage $\omega$ can be regarded as the reduction in the internal material surface [10, 11], an adequate fracture criterion is

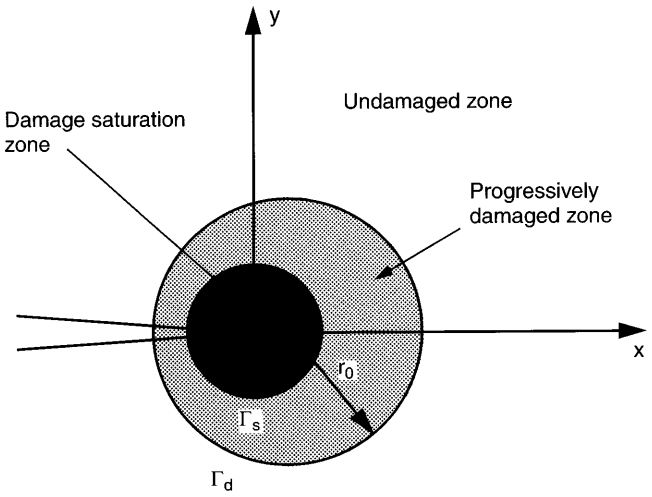


**Fig. 3.** Geometry of damage around a crack tip

$$G_{\text{tip}} = f_{\text{ud}} G_c \quad . \tag{43}$$

Here $G_{\text{tip}}$ is the crack tip energy release rate,

$$G_{\text{tip}} = \frac{1}{\mu_s} K_{\text{tip}}^2 \quad , \tag{44}$$

and $G_c$ is the critical energy release rate of the undamaged material related to the critical stress intensity factor of the virgin material by

$$G_c = \frac{1}{\mu_0} K_c^2 \quad , \tag{45}$$

and $f_{\text{ud}}$ is the area fraction of the undamaged material given by

$$f_{\text{ud}} = 1 - \omega \quad . \tag{46}$$

In the damage saturation region immediately surrounding the crack tip, $\omega = 1 - \mu_s/\mu_0$. Hence,

$$f_{\text{ud}} = \mu_s/\mu_0 \quad . \tag{47}$$

By substituting Eqs. (44–47) into Eq. (43), we obtain the crack initiation condition

$$K_{\text{tip}} = \frac{\mu_s}{\mu_0} K_c \quad . \tag{48}$$

Recalling Eq. (40), the fracture criterion in terms of the applied stress intensity factor $K_{\text{III}}^o$ is

$$K_{\text{III}}^o = \sqrt{\frac{\mu_s}{\mu_0}} K_c \quad . \tag{49}$$

Equation (49) shows that the toughness of the material is lowered by the damage. That is, the shielding effect of the damage is offset by the deterioration effect. The same holds for the mode-I crack problem.

Based on the estimates of elastic moduli of a microcracked solid, the microcrack density and the fraction of microcracked facets, it has been shown [8] from micromechanical analyses that when the damage in the form of microcracking is mainly distributed ahead of the crack tip, it does not contribute to the toughness of the material. Furthermore, the increase in toughness due to crack shielding is essentially counterbalanced by the decrease in toughness due to microcracking [9]. In the framework of continuum damage mechanics it is shown here that damage around a crack tip reduced the toughness of materials. Unlike the approximate estimate [1, 9] an exact expression for the decrease in toughness is given here. The toughness

reduction may be exaggerated by Eq. (44) since the material may not be as severely damaged as that implied by the Kachanov-Lemaitre type damage theory [10, 11]. Of course, additional work is needed to account for the anisotropic damage.

## 4
## Steady-state crack growth

Evans and Fu [1] have shown that a microcracked material exhibits *R*-curve behavior. They calculated the fracture resistance for a steadily growing crack and found that the fracture toughness is higher than that for a stationary crack. They estimated microcrack density, height of the damage zone wake and the peak stresses in the damage zone during crack growth, and attributed the toughness increase to the energy dissipation due to the hysteresis effect (cf. Fig. 1).



We consider the fracture toughness for a steadily slow growing crack under antiplane shear conditions. The energy balance for the crack growth under small scale damage conditions is [1, 15]

$$\frac{1}{\mu_0}(K_{\mathrm{III}}^o)^2 = \frac{1}{\mu_s}K_{\mathrm{tip}}^2 + 2\int_0^{h_s} U^*(\eta)\mathrm{d}\eta + 2\int_{h_s}^{h_0} U^*(\eta)\mathrm{d}\eta \ , \tag{50}$$

where $K_{\mathrm{III}}^o$ is the applied mode-III stress intensity factor (SIF), $K_{\mathrm{tip}}$ is the SIF at the crack tip, $h_s$ and $h_0$ are half the heights of the wakes of saturation and progressive damage zones as shown in Fig. 4, and $U^*(\eta)$ is the residual energy density far behind the growing crack tip

$$U^*(\eta) = \lim_{\xi\to-\infty} U(\xi,\eta) \tag{51a}$$

$$U(\xi,\eta) = \int_0^{\gamma_\alpha} \tau_\alpha \mathrm{d}\gamma_\alpha \tag{51b}$$

In Eqs. (50) and (51), $\xi$ and $\eta$ are the moving Cartesian coordinates at the crack tip

$$\xi = x - a(t), \quad \eta = y \tag{52}$$

where $(x, y)$ are fixed coordinates at the stationary crack tip and $a(t)$ is the crack growth length. We note that $U^*(\eta)$ and $U(\xi,\eta)$ depend on the strain history.

To evaluate integrals in Eq. (50), we need values of $h_s, h_0$ and the distribution of $U^*(\eta)$ in the wake. We assume that the heights $h_s$ and $h_0$ equal the damage zone radii for a stationary crack at crack initiation given in Eqs. (22), (41), (42) and (49), i.e.,

$$h_s = \frac{\mu_s}{\mu_0} r_s = \frac{1}{2\pi}\left(\frac{K_c}{\tau_s}\right)^2 \left(\frac{\mu_s}{\mu_0}\right)^2 \ , \tag{53a}$$

$$h_s = r_0 = \frac{1}{2\pi}\left(\frac{K_c}{\tau_c}\right)^2 \frac{\mu_s}{\mu_0} \ . \tag{53b}$$

The finite element study of crack growth in a microcrack damaged ceramic [4] showed that $h_s$ changes little and the severity of the damage influences $h_0$. Though $h_0$ for a steadily growing

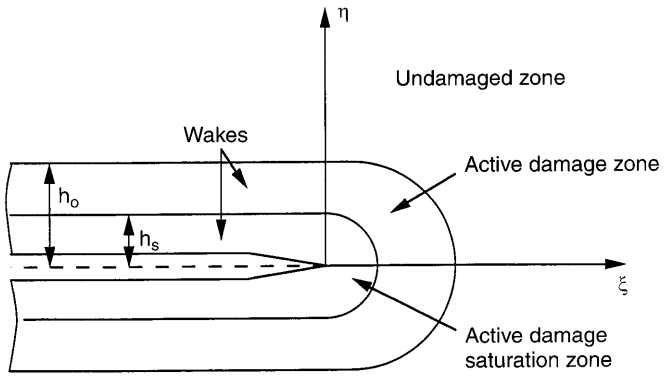


**Fig. 4.** A steadily growing crack and the associated damage zones

crack in a severely damaged ceramic (approximately corresponding to a 90% reduction in Young's modulus) may equal twice of its value at crack initiation, the increase in $h_0$ for moderately damaged ceramics is only moderate. Hence, Eqs. (53) give reasonable values of steady state wake zone heights and will result in conservative predictions of the residual energy.

The residual energy density $U^*(\eta)$ in the wake of saturation zone is the shaded area OABO in Fig. 5a [1]

$$U^*(\eta) = \frac{\tau_c^2}{2\mu_0} - \frac{\tau_s^2}{2\mu_s} + \frac{\tau_c^2}{(1+N)\mu_0}(\beta^{N+1} - 1) \ , \tag{54}$$



and $U^*(\eta)$ in the wake of progressive damage zone is shaded area OACO in Fig. 5b

$$U^*(\eta) = \frac{1-N}{1+N}\frac{\tau_c^2}{2\mu_0}\left\{\left[\frac{\tau_{pk}(\eta)}{\tau_c}\right]^{\frac{N+1}{N}} - 1\right\} \ , \tag{55}$$

where $\tau_{pk}(\eta)$ is the peak stress at height $\eta(= y)$ in the damage zone during crack growth. It is assumed that $\tau_{pk}(\eta) = \max_x\{\tau(x,y)\} = \tau(x_e, y)$, where $\tau(x,y)$ is the stress for the stationary crack. The assumed peak stress will result in a conservative prediction of the residual energy density. Thus the residual energy density in the wake of progressive damage zone can be evaluated by using Eqs. (15), (16) and (36)

$$U^*(\eta) = \frac{1-N}{1+N}\frac{\tau_c^2}{2\mu_0}\left\{\left[\frac{1+N}{4N}\sqrt{(1-N)^2 + 4N\left(\frac{\eta}{h_0}\right)^2} - \frac{(1-N)^2}{4N}\right]^{-1} - 1\right\} \ . \tag{56}$$

Substitution of Eqs. (54) and (56) into Eq. (50) and use of Eq. (53) yield the following relationship between $K_{\text{tip}}$ and $K^o_{\text{III}}$

$$K^o_{\text{III}} = \frac{\mu_0}{\mu_s}K^2_{\text{tip}} + \frac{\mu_s}{\mu_0}FK_c^2 \tag{57}$$

where

$$F = \frac{1}{\pi}\frac{1-N}{1+N}\cdot I \ , \tag{58}$$

$$I = \int_{\frac{\mu_s}{\mu_0}/\left(\frac{\tau_s}{\tau_c}\right)^2}^{1} \frac{(1+N)\sqrt{4Nz^2 + (1-N)^2} + (1-N)^2}{2(1+N)^2z^2 + 2(1-N)^2}\,\mathrm{d}z \tag{59}$$

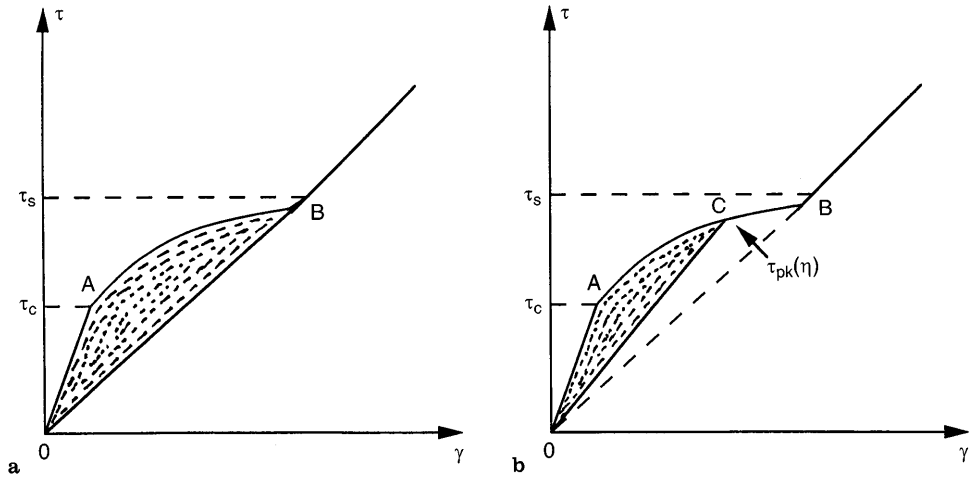


**Fig. 5a,b.** The residual energy density interpreted as the shaded area. **a** In the wake of the saturation zone; **b** in the wake of the progressive damage zone

Since the crack tip damage is given by $\omega = 1 - \mu_s/\mu_0$ for a quasi-statically growing crack, the crack growth condition is still given by Eq. (48). It follows from Eqs. (48) and (57) that

$$\frac{K^o_{\mathrm{III}}}{K_c} = \sqrt{(1+F)\frac{\mu_s}{\mu_0}} \tag{60}$$

and

$$\frac{K_{\mathrm{tip}}}{K^o_{\mathrm{III}}} = \sqrt{\frac{1}{1+F}\frac{\mu_s}{\mu_0}} \tag{61}$$



Figure 6 shows the crack tip SIF, $K_{\mathrm{tip}}$, normalized by the applied SIF, $K^o_{\mathrm{III}}$, versus the shear modulus ratio $\mu_s/\mu_0$. Since $K_{\mathrm{tip}}/K^o_{\mathrm{III}}$ is insensitive to the stress ratio $\tau_s/\tau_c$, the result is shown only for $\tau_s/\tau_c = 1.3$. It is clear that $K_{\mathrm{tip}}/K^o_{\mathrm{III}}$ decreases with a decrease in $\mu_s/\mu_0$. The reduction in the SIF is quite pronounced for smaller values of $\mu_s/\mu_0$. The shielding effect is thus very significant. However, from Fig. 7, where the normalized applied SIF $K^o_{\mathrm{III}}/K_c$, is depicted, we conclude that the applied SIF also decreases with a decrease in $\mu_s/\mu_0$, and the reduction in $K^o_{\mathrm{III}}/K_c$ is as significant as that in $K_{\mathrm{tip}}/K^o_{\mathrm{III}}$. Hence, the crack shielding effect of damage is

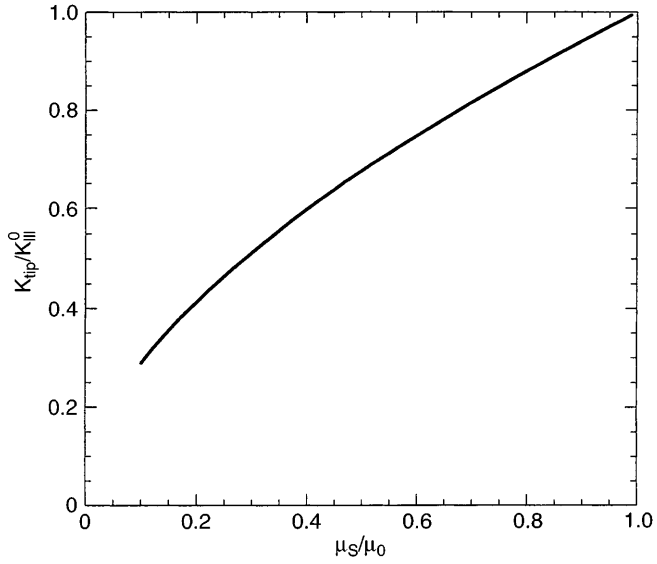


**Fig. 6.** Crack tip stress intensity factor versus shear modulus reduction

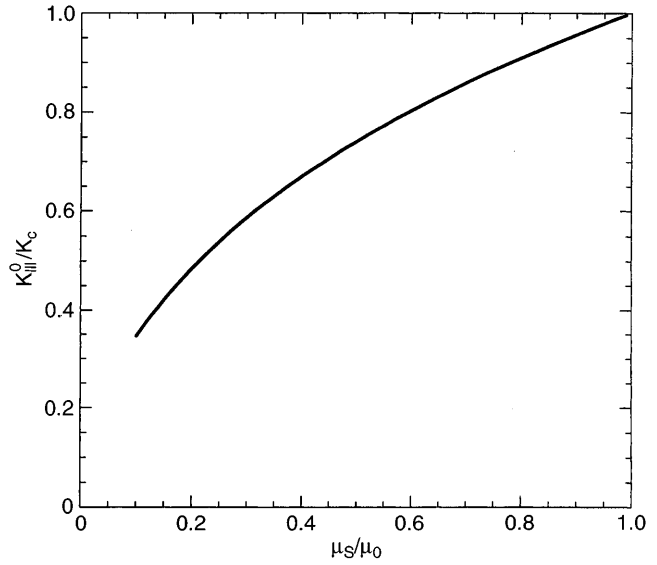


**Fig. 7.** Applied stress intensity factor versus shear modulus reduction

completely offset by the material degradation for a steadily growing crack. We stated earlier that the residual energy is conservatively evaluated. Consequently, the fracture toughness shown in Fig. 7 may be regarded as a lower bound. Recalling that $h_0$ in Eq. (53b) may be undervalued by half for severely damaged ceramics, an approximate value of the upper bound of the toughness is obtained when $F$ in Eq. (60) is replaced by $2F$. The final result deviates from Fig. 7 a little. By using a finite element method fracture resistance of a microcrack damaged solid was calculated [4]. However, the weakening effect of microcracks was not considered and only an $R$-curve behavior referring to the toughness at crack initiation for the microcracking material was predicted. A toughness increase for a steadily growing crack was predicted in [1]. A permanent strain induced by microcracking was assumed in the model, but is neglected herein. Hence, permanent strains may play a key role in microcrack toughening of ceramics. As for stationary cracks, the toughness reduction may be exaggerated by Eq. (60).



## 5
## Concluding remarks

Crack shielding and material degradation in a quasibrittle material have been studied by using a continuum damage model under small-scale damage and antiplane shear conditions. When permanent strains are neglected, a closed form solution for a stationary crack shows that though the crack tip stress intensity is relaxed by the damage, the fracture toughness is actually reduced due to the material degradation, especially when the damage is severe. The same holds for steady crack growth. These results suggest that the damage decreases the fracture resistance of quasibrittle materials when permanent strains are neglected.

## References


1. **Evans, A. G.; Fu, Y.:** Some effects of microcracks on the mechanical properties of brittle solid – II. microcracking toughening. Acta Metall. 33 (1985) 1525–1531
2. **Ortiz, M.:** A continuum theory of crack shielding in ceramics. Trans. ASME J. Appl. Mech. 54 (1987) 54–58
3. **Hutchinson, J. W.:** Crack tip shielding by micro-cracking in brittle solids. Acta Meta. 35 (1987) 1605–1619
4. **Charalambides, P. G.; McMeeking, R. M.:** Finite element method simulation of crack propagation in a brittle microcracking solid. Mech. Mat. 6 (1987) 71–87
5. **Lubarda, V. A.; Krajcinovic, D.:** Tensorial representation of the effective elastic properties of the damage material. Int. J. Damage Mech. 3 (1994) 38–56
6. **Sadowsky, T.:** Mechanical response of semi-brittle ceramics subjected to tension-compression state. Part I: theoretical modeling. Int. J. Damage Mech. 3 (1994) 212–233
7. **Ju, J. W.:** On micromechanical evolutionary damage models for polycrystalline ceramics. Int. J. Damage Mech. 5 (1996) 113–137
8. **Budiansky, B.; O'Connell, R. J.:** Elastic moduli of a cracked solid. Int. J. Solids Struct. 12 (1976) 81–97
9. **Ortiz M.:** Microcrack coalescence and macroscopic crack growth intiation in brittle solids. Int. J. Solids Struct. 24 (1988) 231–250
10. **Kachanov, L. M.:** Introduction to Continuum Damage Mechanics. Dordrecht: M. Nijhoff 1986
11. **Lemaitre, J.:** Coupled elasto-plasticity and damage constitutive equation. Comput. Methods App. Mech. Eng. 51 (1985) 31–49
12. **Mazars, J.:** A description of micro- and macroscale damage of concrete structures. Eng. Fracture Mech. 25 (1986) 729–737
13. **Hult, J. A. H.; McClintock, F. A.:** Elastic-plastic stress and strain distribution around sharp notches under repeated shear. Proc. of 9th Int. Congress of Appl. Mech. Vol. 8, Brussels, Belgium: 1956.
14. **Rice, J. R.:** Stresses due to a sharp notch in a work-hardening elastic-plastic material loaded by longitudinal shear. Trans. ASME, SER E.: J. Appl. Mech. 34 (1967) 287–298
15. **Budiansky, B.; Hutchinson, J. W.; Lambropoulos, J. C.:** Continuum theory of dilatational transformation toughening in ceramics. Int. J. Solids Struct. 19 (1983) 337–355